

# The phonon thermal Hall angle in black phosphorus

Xiaokang Li<sup>1,\*</sup>, Yo Machida<sup>3</sup>, Alaska Subedi<sup>4,5</sup>, Zengwei Zhu<sup>1,\*</sup>, Liang Li<sup>1</sup> and Kamran Behnia<sup>2,\*</sup>

(1) Wuhan National High Magnetic Field Center and School of Physics,  
Huazhong University of Science and Technology, Wuhan 430074, China

(2) Laboratoire de Physique et d'Étude des Matériaux  
(ESPCI - CNRS - Sorbonne Université), PSL Research University, 75005 Paris, France

(3) Department of Physics, Gakushuin University, Tokyo 171-8588, Japan

(4) Centre de Physique Théorique, École Polytechnique,  
CNRS, Université Paris-Saclay, 91128 Palaiseau, France

(5) Collège de France, 11 place Marcelin Berthelot, 75005 Paris, France

(Dated: January 23, 2023)

The origin of phonon thermal Hall Effect (THE) observed in a variety of insulators is yet to be identified. Here, we report on the observation of a thermal Hall conductivity in a non-magnetic elemental insulator, with an amplitude exceeding what has been previously observed. In black phosphorus (BP), the longitudinal ( $\kappa_{ii}$ ), and the transverse,  $\kappa_{ij}$ , thermal conductivities peak at the same temperature and at this peak temperature, the  $\kappa_{ij}/\kappa_{jj}/B$  is  $\approx 10^{-4}$ - $10^{-3}$  T<sup>-1</sup>. Both these features are shared by other insulators displaying THE, despite an absolute amplitude spreading over three orders of magnitude. The absence of correlation between the thermal Hall angle and the phonon mean-free-path imposes a severe constraint for theoretical scenarios of THE. We show that in BP a longitudinal and a transverse acoustic phonon mode anti-cross, facilitating wave-like transport across modes and the anisotropic charge distribution surrounding atomic bonds, paving the way for coupling with magnetic field.

Thermal Hall effect (THE) refers to the emergence of a transverse thermal current by a longitudinal thermal gradient, in presence of a magnetic field. In metals, it is intimately linked to the electrical Hall effect through the Wiedemann-Franz law. Following its original discovery [1], thermal Hall effect was observed in a wide variety of insulating solids [2–10]. Its origin is controversial in exotic cases [11–14], but in strontium titanate [7], a non-magnetic insulator, THE is undoubtedly caused by phonons and is drastically reduced by the introduction of extrinsic atoms [15, 16].

These observations motivated numerous theoretical proposals for a thermal Hall signal produced by heat-carrying phonons [17–25]. They can be broadly classified as either intrinsic (invoking the peculiarities of the phonon spectrum) or extrinsic (referring to consequences of specific phonon scattering mechanisms).

What are the minimal ingredients required to produce a detectable THE? To what extent the effect seen in various families share a common origin? Here, we address these two questions by reporting on the observation of thermal Hall effect in black phosphorus (BP), the simplest insulator known to display THE. It is not only non-magnetic, but also lacking ionic bonds. Interestingly, while the amplitude of the thermal Hall conductivity in BP exceeds what was found in all other insulators, the transverse and the longitudinal thermal conductivities peak at the same temperature and their ratio has a similar amplitude. We note that the charge distribution is anisotropic and atomic vibrations can therefore respond to the magnetic field. We show that two out of the three acoustic branches anti-cross and are close to degeneracy in the momentum space, and therefore, energy transfer across harmonic vibrational states [26, 27] plays a role in

setting the amplitude of thermal conductivity and since the charge distribution is anisotropic, magnetic field can couple to atomic vibrations. The austere context of our experimental observation strongly constrains theoretical scenarios.

Bulk black phosphorus is a stack of puckered honeycomb layers [28, 29] (Figure 1A). Phosphorus atoms have two distinct sites marked in blue and red. The  $x$ - and  $z$ -axes correspond to the armchair and zigzag directions of the BP layer plane, following the convention used in ref [30]. The experimental set-up is shown in Figure 1B (See the supplement [31] for details). Figure 1C displays the temperature dependence of the longitudinal thermal conductivity. As found in previous studies [32, 33], there is a large anisotropy.  $\kappa_{xx}$  peaks to  $311$  WK<sup>-1</sup>m<sup>-1</sup> at 27 K and  $\kappa_{zz}$  to  $1770$  WK<sup>-1</sup>m<sup>-1</sup> at 34 K. This is a consequence of the larger sound velocity along the zigzag direction.

The field dependent thermal Hall angle  $\nabla T_j/\nabla T_i$ , is shown in Figure 1D and E for two different configurations and at four different temperatures. In both configurations, it is linear in magnetic field. Interestingly,  $\nabla T_j/\nabla T_i$  is anisotropic: It attains  $5.0 \times 10^{-3}$  at 12 T and 35.3 K for one configuration and  $1.2 \times 10^{-3}$  at 12 T and 32.1 K for the other. This fourfold anisotropy is clearly seen in the temperature dependence of  $\nabla T_j/\nabla T_i$  (Figure 1F).

Combining the thermal Hall angle (Figure 1F), the longitudinal thermal conductivity (Figure 1C), leads us to the thermal Hall conductivity, shown in Figure 2A. The inset shows the contribution of electrons to THE can be estimated through the Wiedemann-Franz law. At low temperatures,  $\kappa_{ij}^e \approx L_0 \sigma_{ij} T \ll \kappa_{ij}$  and therefore electrons can be totally neglected below 50 K and

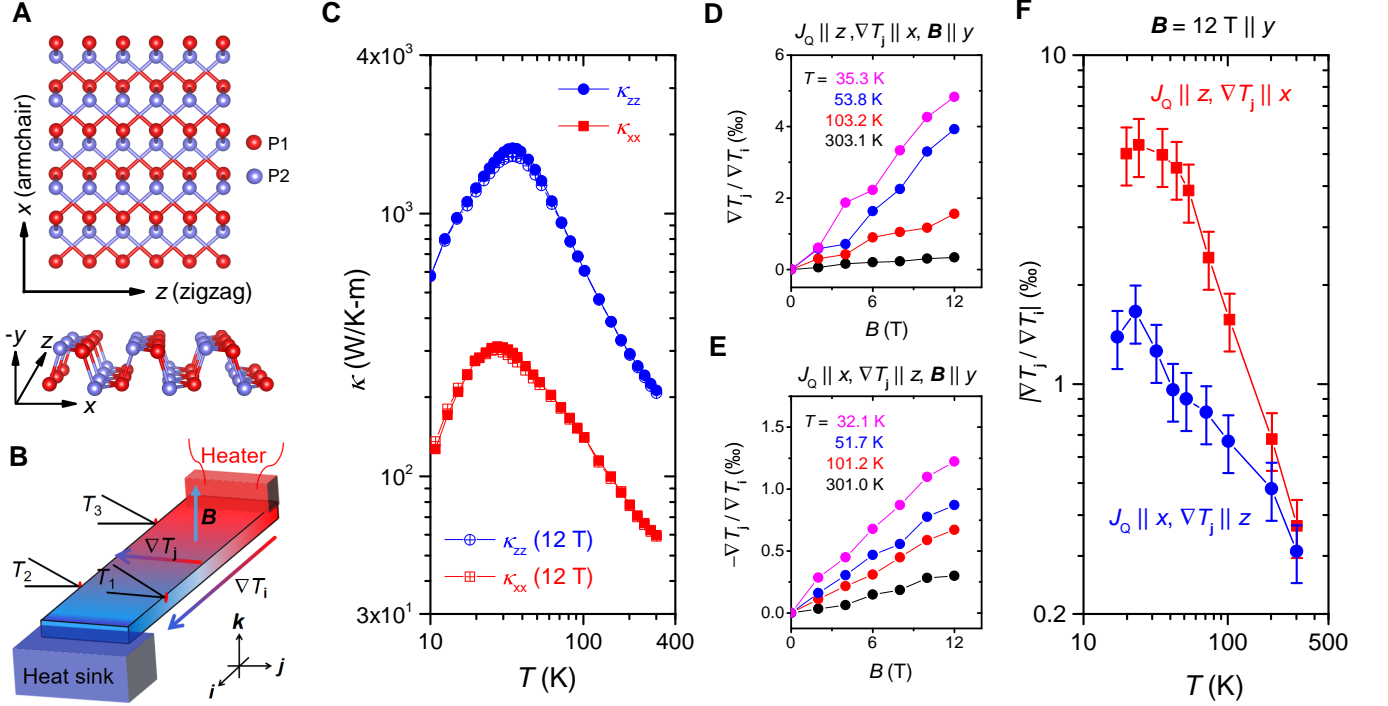


FIG. 1. **Lattice structure, set-up and thermal transport** (A) Top (two layers) and side (single layer) view of the lattice of black phosphorus (BP). P atoms, marked in blue and red, along with atomic sites with distinct environments. The  $x$  and  $z$  axes respectively correspond to the armchair and zigzag directions of the BP layer plane. (B) The setup for measuring longitudinal and transverse thermal conductivities. (C) Thermal conductivity along the armchair ( $\kappa_{xx}$ ) and the zigzag ( $\kappa_{zz}$ ) orientations. There is a large in-plane anisotropy, as found by previous studies [32, 33]. (D-E) Field dependence of the thermal Hall angle at different temperatures with the heat current  $J_Q$  along the  $z(x)$ -axis, and the transverse temperature gradient along the  $x(z)$ -axis. In both cases, the magnetic field  $B$  is along the  $y$ -axis. (F) The temperature dependence of the thermal Hall angle for two different configurations at 12 T.

near the peaks in thermal conductivities. Strikingly,  $\kappa_{zx}$  and  $-\kappa_{xz}$  become very close to each other. Within experimental margin, they are equal, as expected by the Onsager reciprocal relations for diffusive transport ( $\kappa_{ij}(H) = \kappa_{ji}(-H) = -\kappa_{ji}(H)$ ) [1, 40]. The inequality between the two off-diagonal components at high temperature can be tracked to the gradual emergence of a sizeable thermoelectric response at high temperature and therefore, a significant difference between the measured thermal conductivity (in absence of charge current) and the true Onsager coefficient (which is thermal conductivity in absence of the electric field). A similar phenomenon was observed in the case of dilute metallic strontium titanate [16] (See Supplemental material [31] for details).

Figure 2B and C compare the temperature dependence of longitudinal and transverse thermal conductivity. Multiplying  $\kappa_{xz}(T)$  and  $\kappa_{zx}(T)$  by a factor of -150 and 1000 respectively, one finds that  $\kappa_{ij}(T)$  and  $\kappa_{ii}(T)$  peak almost at the same temperature for both configurations. It's worth noting that the  $\kappa_{ij}/\kappa_{ii}$  ratio is anisotropic. This is unavoidable and due to the combination of the Onsager reciprocity ( $\kappa_{ij} = -\kappa_{ji}$ ) and the anisotropy of longitudinal thermal conductivity ( $\kappa_{ii} \neq$

$\kappa_{jj}$ ).

Let us now compare BP with other insulators. The peak amplitude of  $\kappa_{ij}$  in BP  $\sim 2.2 \text{ WK}^{-1}\text{m}^{-1}$  is four orders of magnitude larger than what was seen in  $\text{Tb}_3\text{Ga}_3\text{O}_{12}$  [1], almost two orders of magnitude larger than the values reported for cuprates [5, 6] and  $\text{SrTiO}_3$  [7], and almost twice what was recently reported in  $\text{Cu}_3\text{TeO}_6$  [9]. On the other hand, the thermal Hall angle remains in the same narrow range of 0.1-1% under a magnetic field of about 10 T. As seen in Figure 2D, across several orders of magnitude variation, longitudinal and transverse thermal conductivity scale with each other. Using, the magnetic length,  $\ell_B = \sqrt{\hbar/eB}$  one can extract a length scale,  $\lambda_{tha}$ , from this angle:  $\lambda_{tha}^2/\ell_B^2 = \kappa_{ij}/\kappa_{jj}$ . In the case of electrons in the weak-field limit, extracting a length in this way from the Hall angle will give rise to a geometric average of the mean-free-path and the Fermi wavelength. In a similar manner, in some scenarios for phonon Hall response, one expects a correlation between the Hall angle and the mean-free-path.

Intriguingly, for all these solids,  $\lambda_{tha}$  remains between 2 and 7 angstroms. Such a length is comparable to the shortest possible phonon wavelength allowed by the in-

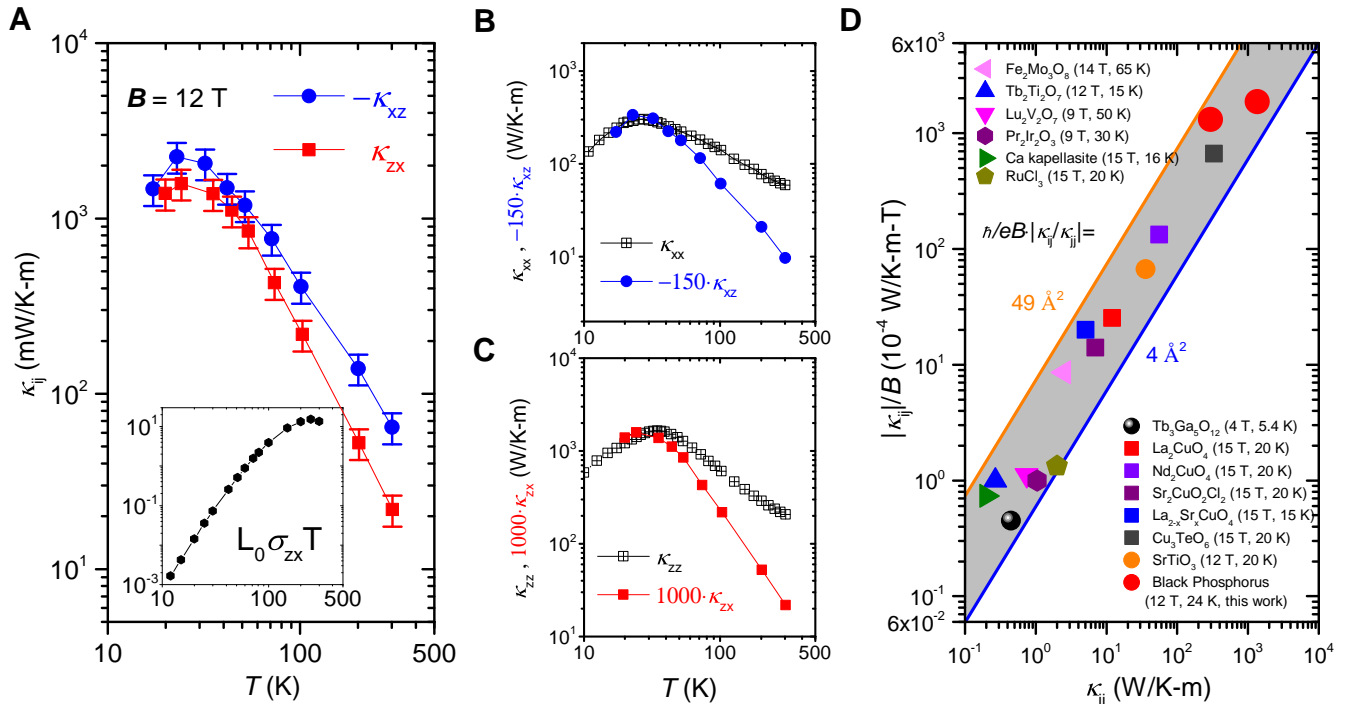


FIG. 2. **Thermal Hall conductivity** (A) Temperature dependence of the measured off-diagonal thermal conductivities,  $\kappa_{zx}$  and  $-\kappa_{xz}$ . At low temperature, they become equal to each other within experimental margin, as expected by Onsager reciprocity. With warming towards room temperature a difference arises, presumably due to non-negligible contribution of the thermoelectric response to transverse heat flow. (B) Comparison of the temperature dependence of  $\kappa_{xx}$ , multiplied by  $-150$  and  $\kappa_{xz}$ . (C) Comparison of the temperature dependence of  $\kappa_{zx}$ , multiplied by  $1000$  and  $\kappa_{zz}$ . Note that they all peak almost at the same temperature. (D) Comparison of the transverse  $\kappa_{ij}/B$  and the longitudinal  $\kappa_{jj}$  thermal conductivity in different insulators (source: [1, 3, 5–7, 9, 10, 14, 34–36]). Even though the longitudinal thermal conductivity  $\kappa_{jj}$  varies by 4 orders of magnitude, their ratio  $\kappa_{ij}/\kappa_{jj}/B$  remains within the range of  $\approx 10^{-4}$ – $10^{-3}$  T $^{-1}$ . The length scale  $\lambda_{tha} = \ell_B \cdot \sqrt{\kappa_{ij}/\kappa_{jj}}$  remains between 2 and 7 Å, equivalent to the shortest phonon wavelength allowed by the distance between atoms.

teratomic distance. Our observation that it does not correlate with the phonon mean-free-path, which varies by more than three orders of magnitude among these solids, excludes many (but not all) ‘extrinsic’ scenarios.

A second universal feature is shown in Figure 3. As first noted in ref. [7], the transverse and longitudinal conductivities occur peak almost the same temperature in all insulators displaying THE. Thus, the thermal Hall response is always maximal when the wave-vector of the heat-carrying acoustic phonons have sufficiently shrunk to make Umklapp scattering irrelevant, but boundary scattering is not yet the dominant scattering mechanisms.

Even in the case of BP, ‘extrinsic’ scenarios cannot be excluded. Since the inversion center is not at an atomic site, a vacancy breaks the local inversion center and can generate skew scattering or side jump’. In the scenario put forward by Guo *et al.* [25], resonant coupling between phonons and dynamical effects, generates a ‘side jump’ thermal Hall effect, where the thermal Hall angle does not scale with longitudinal thermal conductivity, in agreement with experiments. However, the suppression of THE by the introduction of extrinsic atoms in strontium titanate [15, 16] and the absence of correlation

between the thermal Hall angle and the phonon mean-free-path constitute serious challenges for any ‘extrinsic’ scenario.

Let us now consider those features of BP, which can nourish an ‘intrinsic’ scenario. The phonon spectrum of BP [37] with a focus on energies below 100 cm $^{-1}$  is shown in Figure 4A. At 30 K, only the three acoustic modes (one longitudinal and two transverse) are thermally populated. Figure 4B shows the angle dependence of their wave-vector with an energy of  $k_B T_{peak} \approx 20$  cm $^{-1}$ , which roughly corresponds to the peak temperature. As seen in the figure, two acoustic modes, the longitudinal (LA) and a transverse mode (TA1) display a pronounced anti-crossing and become almost degenerate along the  $z$ -axis.

A second relevant feature is the spatial distribution of charge density in bulk BP. Computed and highlighted by Hu *et al.* [39] (See Figure 4C), it is highly orientational. We also note that dipole-active phonon modes have been observed in BP by infrared spectroscopy [41], suggesting the presence of unevenly distributed positive and negative charges. Therefore, even in this covalent solid, the magnetic field can couple to phonons through its influence on charge distribution. Interestingly, Vala-

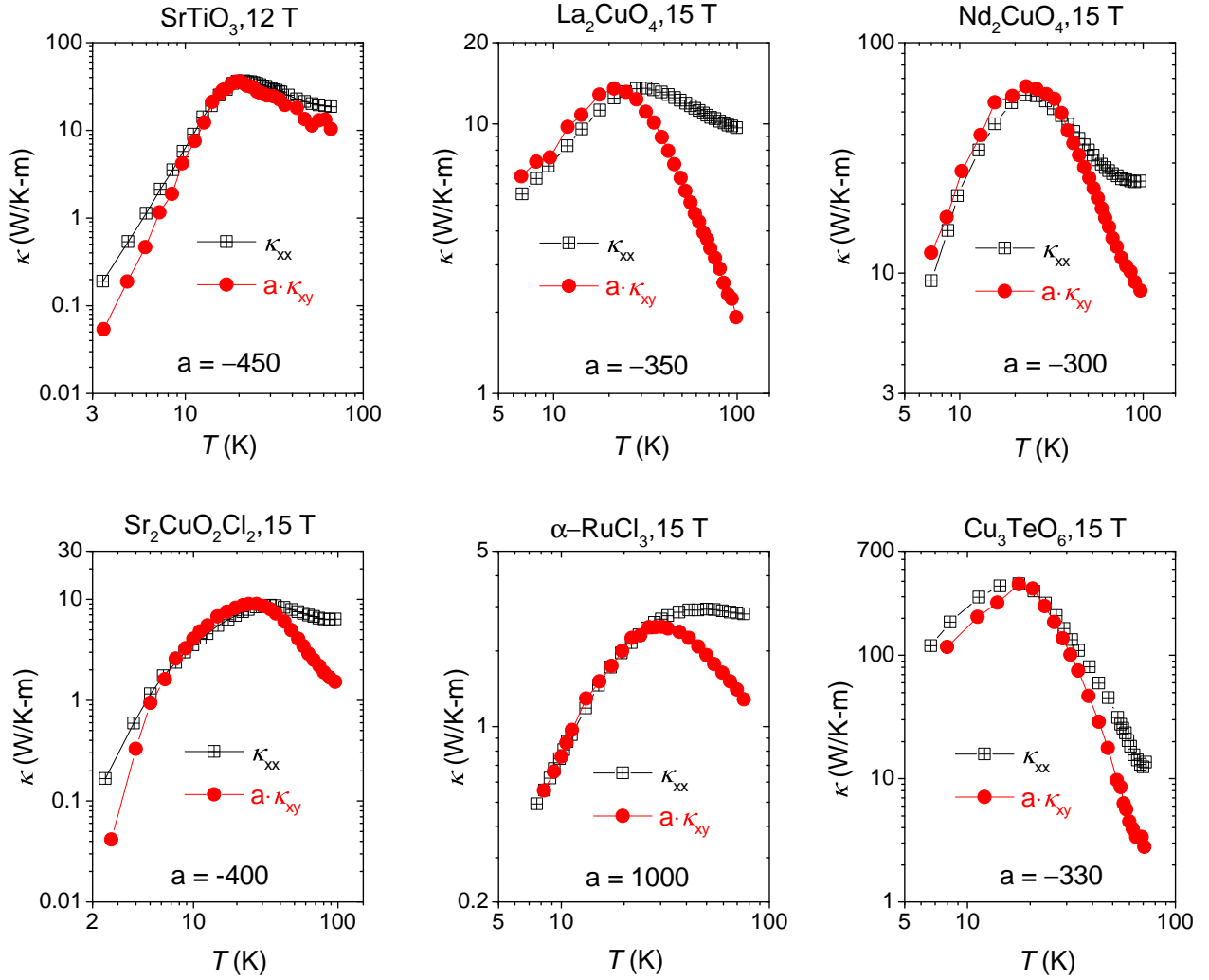


FIG. 3. **Peaks in  $\kappa_{ij}(T)$  and in  $\kappa_{ii}(T)$ .** Comparison of  $\kappa_{ij}(T)$  with  $\kappa_{ii}(T)$  in six different insulating materials: SrTiO<sub>3</sub> [7], La<sub>2</sub>CuO<sub>4</sub> [6], Nd<sub>2</sub>CuO<sub>4</sub> [6], Sr<sub>2</sub>CuO<sub>2</sub>Cl<sub>2</sub> [6],  $\alpha$ -RuCl<sub>3</sub> [13] and Cu<sub>3</sub>TeO<sub>6</sub> [9]. In each case,  $\kappa_{ij}(T)$  is multiplied by an amplification factor  $a$  varying from (-)300 to (-)1000.

giannopoulos *et al.* [42] have found that there is a remarkable anisotropy of electromagnetic propagation in black P. They calculated the real and imaginary parts of the dielectric constant and found that an electromagnetic wave is damped much less along the ‘zigzag’ direction than along the ‘armchair direction’ (See the supplement for details [31]).

Note that at peak temperature, the phonon mean-free-path is well below the sample thickness (See supplement [31]), implying another source of thermal resistivity on top of boundary scattering. Inter-branch coupling between harmonic vibrations was recently invoked to explain the glass-like thermal conductivity of many crystalline solids [26, 27]. Our result calls for a theoretical examination of the role of magnetic field in such a context.

In magnetic insulators, collective excitations may cou-

ple to phonons and generate a thermal Hall effect [24]. In contrast, in BP, as well as in strontium titanate, phonons are the only identified collective excitations. The two solids share at least two uncommon features. In both, the phonon mean-free-path is not a monotonous function of temperature, which has been tracked to abundance of momentum-conserving phonon-phonon collisions [37, 43]. In both, there is a non-trivial coupling between distinct phonon modes [44].

In summary, phonons of black phosphorus generate a  $\kappa_{ij}$  larger than what was reported in any other insulator. The ratio of  $\kappa_{ij}$  to  $\kappa_{jj}$  in this system is comparable to other insulators and in all cases, the longitudinal and transverse thermal conductivities peak at the same temperature where the phonon wavelength and the magnetic length are comparable in size. The result shortens list of ingredients required to produce a phonon THE.

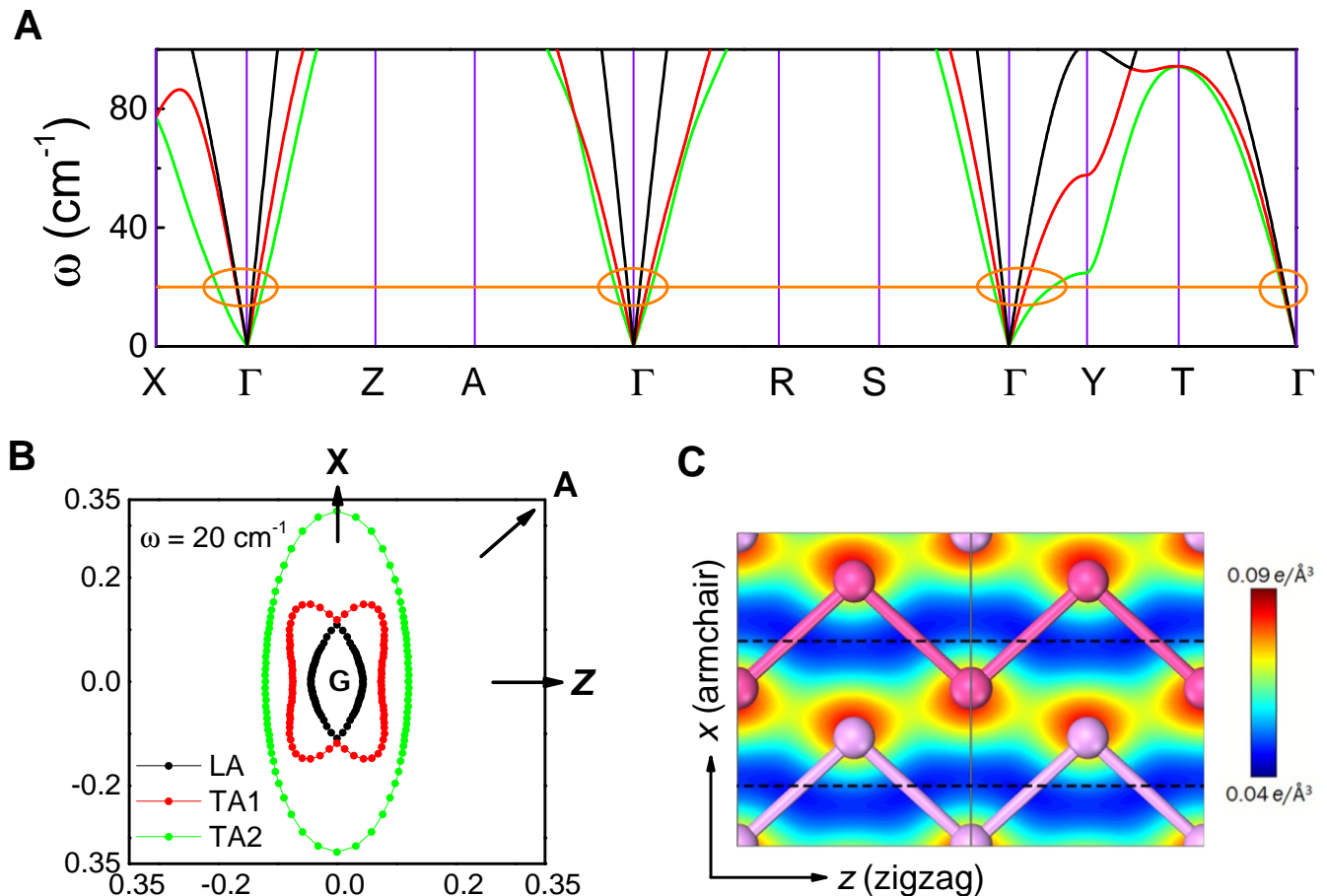


FIG. 4. **Phonons in black phosphorus** (A) Calculated phonon spectrum [37] below  $100 \text{ cm}^{-1}$ . The three acoustic branches are plotted with different colors. This spectrum, first calculated in ref. [37] is in agreement with a recent X-ray experimental study [38]. (B) Angle dependence of the phonon wave-vectors with a frequency of  $20 \text{ cm}^{-1}$  projected in the  $xz$  plane. The longitudinal mode (in black) and a transverse mode (in red) are almost degenerate along  $x$ . Energy transfer across phonon branches can be affected by the magnetic field. (C) Spatial distribution of charge concentration in bulk BP [39]. Note the  $x$ - $z$  anisotropy.

**Data availability:** The data that support the findings of this study are available from the corresponding author upon reasonable request.

\* lixiaokang@hust.edu.cn

\* zengwei.zhu@hust.edu.cn

\* Kamran.Behnia@espci.fr

- 
- [1] C. Strohm, G. L. J. A. Rikken, and P. Wyder, Phenomenological evidence for the phonon Hall effect, *Phys. Rev. Lett.* **95**, 155901 (2005).
- [2] M. Hirschberger, J. W. Krizan, R. J. Cava, and N. P. Ong, Large thermal Hall conductivity of neutral spin excitations in a frustrated quantum magnet, *Science* **348**, 106 (2015).
- [3] T. Ideue, T. Kurumaji, S. Ishiwata, and Y. Tokura, Giant thermal Hall effect in multiferroics, *Nature Materials* **16**, 797 (2017).
- [4] K. Sugii, M. Shimozawa, D. Watanabe, Y. Suzuki, M. Halim, M. Kimata, Y. Matsumoto, S. Nakatsuji, and M. Yamashita, Thermal Hall effect in a phonon-glass  $\text{Ba}_3\text{CuSb}_2\text{O}_9$ , *Phys. Rev. Lett.* **118**, 145902 (2017).
- [5] G. Grissonnanche, S. Thériault, A. Gourgout, M.-E. Boulanger, E. Lefrançois, A. Ataei, F. Laliberté, M. Dion, J.-S. Zhou, S. Pyon, *et al.*, Chiral phonons in the pseudogap phase of cuprates, *Nature Physics* **16**, 1108 (2020).
- [6] M.-E. Boulanger, G. Grissonnanche, S. Badoux, A. Lalire, É. Lefrançois, A. Legros, A. Gourgout, M. Dion, C. Wang, X. Chen, *et al.*, Thermal Hall conductivity in the cuprate mott insulators  $\text{Nd}_2\text{CuO}_4$  and  $\text{Sr}_2\text{CuO}_2\text{Cl}_2$ ,

- Nature Communications **11**, 1 (2020).
- [7] X. Li, B. Fauqué, Z. Zhu, and K. Behnia, Phonon thermal Hall effect in strontium titanate, *Phys. Rev. Lett.* **124**, 105901 (2020).
- [8] M. Akazawa, M. Shimozawa, S. Kittaka, T. Sakakibara, R. Okuma, Z. Hiroi, H.-Y. Lee, N. Kawashima, J. H. Han, and M. Yamashita, Thermal Hall effects of spins and phonons in kagome antiferromagnet Cd-Kapellasite, *Phys. Rev. X* **10**, 041059 (2020).
- [9] L. Chen, M.-E. Boulanger, Z.-C. Wang, F. Tafti, and L. Taillefer, Large phonon thermal Hall conductivity in the antiferromagnetic insulator  $\text{Cu}_3\text{TeO}_6$ , *Proceedings of the National Academy of Sciences* **119**, e2208016119 (2022).
- [10] T. Uehara, T. Ohtsuki, M. Udagawa, S. Nakatsuji, and Y. Machida, Phonon thermal Hall effect in a metallic spin ice, *Nature Communications* **13**, 1 (2022).
- [11] Y. Kasahara, T. Ohnishi, Y. Mizukami, O. Tanaka, S. Ma, K. Sugii, N. Kurita, H. Tanaka, J. Nasu, Y. Motome, *et al.*, Majorana quantization and half-integer thermal quantum Hall effect in a kitaev spin liquid, *Nature* **559**, 227 (2018).
- [12] R. Hentrich, M. Roslova, A. Isaeva, T. Doert, W. Brenig, B. Büchner, and C. Hess, Large thermal Hall effect in  $\alpha\text{-RuCl}_3$ : Evidence for heat transport by Kitaev-Heisenberg paramagnons, *Phys. Rev. B* **99**, 085136 (2019).
- [13] E. Lefrançois, G. Grissonnanche, J. Baglo, P. Lampen-Kelley, J.-Q. Yan, C. Balz, D. Mandrus, S. E. Nagler, S. Kim, Y.-J. Kim, N. Doiron-Leyraud, and L. Taillefer, Evidence of a phonon Hall effect in the Kitaev spin liquid candidate  $\alpha\text{-RuCl}_3$ , *Phys. Rev. X* **12**, 021025 (2022).
- [14] J. Bruin, R. Claus, Y. Matsumoto, N. Kurita, H. Tanaka, and H. Takagi, Robustness of the thermal Hall effect close to half-quantization in  $\alpha\text{-RuCl}_3$ , *Nature Physics* **18**, 401 (2022).
- [15] S. Sim, H. Yang, H.-L. Kim, M. J. Coak, M. Itoh, Y. Noda, and J.-G. Park, Sizable suppression of thermal Hall effect upon isotopic substitution in  $\text{SrTiO}_3$ , *Phys. Rev. Lett.* **126**, 015901 (2021).
- [16] S. Jiang, X. Li, B. Fauqué, and K. Behnia, Phonon drag thermal Hall effect in metallic strontium titanate, *Proceedings of the National Academy of Sciences* **119**, e2201975119 (2022).
- [17] L. Sheng, D. N. Sheng, and C. S. Ting, Theory of the phonon Hall effect in paramagnetic dielectrics, *Phys. Rev. Lett.* **96**, 155901 (2006).
- [18] Y. Kagan and L. A. Maksimov, Anomalous Hall effect for the phonon heat conductivity in paramagnetic dielectrics, *Phys. Rev. Lett.* **100**, 145902 (2008).
- [19] L. Zhang, J. Ren, J.-S. Wang, and B. Li, Topological nature of the phonon Hall effect, *Phys. Rev. Lett.* **105**, 225901 (2010).
- [20] T. Qin, J. Zhou, and J. Shi, Berry curvature and the phonon Hall effect, *Phys. Rev. B* **86**, 104305 (2012).
- [21] B. K. Agarwalla, L. Zhang, J.-S. Wang, and B. Li, Phonon Hall effect in ionic crystals in the presence of static magnetic field, *The European Physical Journal B* **81**, 197 (2011).
- [22] J.-Y. Chen, S. A. Kivelson, and X.-Q. Sun, Enhanced thermal Hall effect in nearly ferroelectric insulators, *Phys. Rev. Lett.* **124**, 167601 (2020).
- [23] B. Flebus and A. H. MacDonald, Charged defects and phonon Hall effects in ionic crystals, *Phys. Rev. B* **105**, L220301 (2022).
- [24] L. Mangeolle, L. Balents, and L. Savary, Phonon Thermal Hall Conductivity from Scattering with Collective Fluctuations, arXiv:2206.06183 (2022).
- [25] H. Guo, D. G. Joshi, and S. Sachdev, Resonant thermal Hall effect of phonons coupled to dynamical defects, *Proceedings of the National Academy of Sciences* **119**, e2215141119 (2022).
- [26] M. Simoncelli, N. Marzari, and F. Mauri, Unified theory of thermal transport in crystals and glasses, *Nature Physics* **15**, 809 (2019).
- [27] L. Isaeva, G. Barbalinardo, D. Donadio, and S. Baroni, Modeling heat transport in crystals and glasses from a unified lattice-dynamical approach, *Nature Communications* **10**, 3853 (2019).
- [28] L. Li, Y. Yu, G. J. Ye, Q. Ge, X. Ou, H. Wu, D. Feng, X. H. Chen, and Y. Zhang, Black phosphorus field-effect transistors, *Nature Nanotechnology* **9**, 372 (2014).
- [29] X. Ling, H. Wang, S. Huang, F. Xia, and M. S. Dresselhaus, The renaissance of black phosphorus, *Proceedings of the National Academy of Sciences* **112**, 4523 (2015).
- [30] X. Ling, S. Huang, E. H. Hasdeo, L. Liang, W. M. Parkin, Y. Tsumi, A. R. Nugraha, A. A. Puzos, P. M. Das, B. G. Sumpter, *et al.*, Anisotropic electron-photon and electron-phonon interactions in black phosphorus, *Nano Letters* **16**, 2260 (2016).
- [31] See Supplemental Material for more details (2022).
- [32] Y. Wang, G. Xu, Z. Hou, B. Yang, X. Zhang, E. Liu, X. Xi, Z. Liu, Z. Zeng, W. Wang, *et al.*, Large anisotropic thermal transport properties observed in bulk single crystal black phosphorus, *Applied Physics Letters* **108**, 092102 (2016).
- [33] B. Sun, X. Gu, Q. Zeng, X. Huang, Y. Yan, Z. Liu, R. Yang, and Y. K. Koh, Temperature dependence of anisotropic thermal-conductivity tensor of bulk black phosphorus, *Advanced Materials* **29**, 1603297 (2017).
- [34] G. Grissonnanche, A. Legros, S. Badoux, E. Lefrançois, V. Zlatoski, M. Lizaire, F. Laliberté, A. Gourgout, J.-S. Zhou, S. Pyon, *et al.*, Giant thermal Hall conductivity in the pseudogap phase of cuprate superconductors, *Nature* **571**, 376 (2019).
- [35] Y. Onose, T. Ideue, H. Katsura, Y. Shiomi, N. Nagaosa, and Y. Tokura, Observation of the magnon Hall effect, *Science* **329**, 297 (2010).
- [36] H. Doki, M. Akazawa, H.-Y. Lee, J. H. Han, K. Sugii, M. Shimozawa, N. Kawashima, M. Oda, H. Yoshida, and M. Yamashita, Spin thermal Hall conductivity of a kagome antiferromagnet, *Phys. Rev. Lett.* **121**, 097203 (2018).
- [37] Y. Machida, A. Subedi, K. Akiba, A. Miyake, M. Tokunaga, Y. Akahama, K. Izawa, and K. Behnia, Observation of poiseuille flow of phonons in black phosphorus, *Science Advances* **4**, eaat3374 (2018).
- [38] E. A. A. Pogna, A. Bosak, A. Chumakova, V. Milman, B. Winkler, L. Viti, and M. S. Vitiello, Lattice dynamics and elastic properties of black phosphorus, *Phys. Rev. B* **105**, 184306 (2022).
- [39] Z.-X. Hu, X. Kong, J. Qiao, B. Normand, and W. Ji, Interlayer electronic hybridization leads to exceptional thickness-dependent vibrational properties in few-layer black phosphorus, *Nanoscale* **8**, 2740 (2016).
- [40] H. B. G. Casimir, On Onsager's principle of microscopic reversibility, *Rev. Mod. Phys.* **17**, 343 (1945).
- [41] S. Sugai and I. Shirovani, Raman and infrared reflection

- spectroscopy in black phosphorus, *Solid State Communications* **53**, 753 (1985).
- [42] C. A. Valagiannopoulos, M. Mattheakis, S. N. Shirodkar, and E. Kaxiras, Manipulating polarized light with a planar slab of black phosphorus, *Journal of Physics Communications* **1**, 045003 (2017).
- [43] V. Martelli, J. L. Jiménez, M. Continentino, E. Baggio-Saitovitch, and K. Behnia, Thermal transport and phonon hydrodynamics in strontium titanate, *Phys. Rev. Lett.* **120**, 125901 (2018).
- [44] B. Fauqué, P. Bourges, A. Subedi, K. Behnia, B. Baptiste, B. Roessli, T. Fennell, S. Raymond, and P. Steffens, Mesoscopic fluctuating domains in strontium titanate, *Phys. Rev. B* **106**, L140301 (2022).
- [45] S. Baroni, S. de Gironcoli, A. Dal Corso, and P. Giannozzi, Phonons and related crystal properties from density-functional perturbation theory, *Rev. Mod. Phys.* **73**, 515 (2001).
- [46] P. Giannozzi, S. Baroni, N. Bonini, M. Calandra, R. Car, C. Cavazzoni, D. Ceresoli, G. L. Chiarotti, M. Cococcioni, I. Dabo, *et al.*, QUANTUM ESPRESSO: a modular and open-source software project for quantum simulations of materials, *Journal of Physics: Condensed Matter* **21**, 395502 (2009).
- [47] J. P. Perdew, K. Burke, and M. Ernzerhof, Generalized gradient approximation made simple, *Phys. Rev. Lett.* **77**, 3865 (1996).
- [48] K. F. Garrity, J. W. Bennett, K. M. Rabe, and D. Vanderbilt, Pseudopotentials for high-throughput DFT calculations, *Computational Materials Science* **81**, 446 (2014).
- [49] S. Grimme, Semiempirical GGA-type density functional constructed with a long-range dispersion correction, *Journal of Computational Chemistry* **27**, 1787 (2006).
- [50] T. Nagahama, M. Kobayashi, Y. Akahama, S. Endo, and S.-i. Narita, Optical determination of dielectric constant in black phosphorus, *Journal of the Physical Society of Japan* **54**, 2096 (1985).

### Acknowledgements

We thank Bruce Normand and Wei Ji for authorizing us to use Figure 4A. This work was supported by The National Key Research and Development Program of China (Grant No.2022YFA1403500), the National Science Foundation of China (Grant No. 11574097 and No. 51861135104) and the Fundamental Research Funds for the Central Universities (Grant no. 2019kfyXMBZ071). Y. M. acknowledges funding from Grants-in-Aid for Scientific Research (Grant No. 19H01840). A. S. acknowledges computational resources provided by GENCI-TGCC (grant A0130913028). K. B. was supported by the Agence Nationale de la Recherche (ANR-19-CE30-0014-04). X. L. acknowledges the China National Postdoctoral Program for Innovative Talents (Grant No.BX20200143) and the China Postdoctoral Science Foundation (Grant No.2020M682386).

**Supplemental Material for “The phonon thermal Hall angle in black phosphorus” by X. Li et al.**

**S1. MATERIALS AND METHODS**

Black phosphorus crystals synthesized under high pressure came from two different sources. Samples #1-1, #1-2, #1-3, cut and cleaved from the same mother crystal, were obtained commercially. Samples #2-1, #2-2, also cut and cleaved from the same mother crystal, provided by Prof. Yuichi Akahama (University of Hyogo). Samples #1-1, #2-1 and #2-2 were used for thermal transport measurements, the samples #1-2, #1-3 were used for electrical transport measurements. The details of all samples are listed in Table S1.

sample	$l_x$ (mm)	$l_z$ (mm)	$l_y$ (mm)	measurements
#1-1	1.3	0.7	0.03	$\kappa_{xx}, \kappa_{zz}, \kappa_{xz}, \kappa_{zx}$
#1-2	0.6	0.7	0.02	$\rho_{zz}, \rho_{zx}$
#1-3	0.8	0.7	0.02	$\rho_{xx}$
#2-1	0.85	2.5	0.035	$\kappa_{zz}, \kappa_{zx}$
#2-2	3.0	1.3	0.07	$\kappa_{xx}, \kappa_{xz}$

TABLE S1. Details of black phosphorus samples used in this work.

All transport experiments were performed in a commercial measurement system (Quantum Design PPMS) within a stable high-vacuum sample chamber. Electrical transport responses were measured by a standard four-probe method using a current source (Keithley6221) and a DC-nanovoltmeter (Keithley2182A). In thermal transport measurements, both one-heater-three-thermocouples (type E) and one-heater-three-thermometers (Cernox 1030) techniques were employed to simultaneously measure the longitudinal and transverse thermal gradient. The thermal gradient in the sample was produced through a 4.7 k $\Omega$  chip resistor alimented by a current source (Keithley6221). The DC voltage on the heater and thermocouples (thermometers) was measured through the DC-nanovoltmeter (Keithley2182A). The thermocouples, the heat-sink, and the heater were connected to samples directly or by gold wires with a 50 microns diameter. All contacts on the sample were made using silver paste.

The longitudinal ( $\nabla T_i = (T_3 - T_2)/l$ ) and the transverse ( $\nabla T_j = (T_1 - T_2)/w$ ) thermal gradient generated by a longitudinal thermal current  $J_Q$  were measured. They lead to the longitudinal ( $\kappa_{ii}$ ) and the transverse ( $\kappa_{ij}$ ) thermal conductivity, as well as the thermal Hall angle ( $\nabla T_j / \nabla T_i$ ):

$$\kappa_{ii} = \frac{Q_i}{\nabla T_i} \quad (\text{S1})$$

$$\frac{\nabla T_j}{\nabla T_i} = \frac{\kappa_{ij}}{\kappa_{jj}} \quad (\text{S2})$$

$$\kappa_{ij} = \frac{\nabla T_j}{\nabla T_i} \cdot \kappa_{jj} \quad (\text{S3})$$

Here  $l$ ,  $w$ ,  $Q$  are the distance between longitudinal thermocouples, the sample width and the heat power respectively.

The phonon dispersions were obtained using the dynamical matrices calculated in Ref. [37]. These calculations were performed using density functional perturbation theory [45] as implemented in the QUANTUM ESPRESSO package [46]. The Perdew, Burke, and Ernzerhof’s generalized gradient approximation [47] and Garrity et al.’s pseudopotentials [48] were used. The van der Waals interaction was taken into account using Grimme’s semiempirical recipe [49]. Planewave cutoffs of 50 and 250 Ry were used for the basis-set and charge density expansions, respectively. A  $12 \times 12 \times 12$   $k$ -point grid was used for the Brillouin zone integration in the self-consistent density functional theory calculations with a Marzari-Vanderbilt smearing of 0.02 Ry. The dynamical matrices were calculated on an  $8 \times 8 \times 8$   $q$ -point grid, and the phonon dispersions and density of states were obtained by Fourier interpolation.

**S2. PROCESSING THE RAW DATA**

Figure S1A shows the longitudinal and transverse temperature difference of sample #2-1 at 102 K under a heat power of 15.7 mW. With the field sweeping from -12 T to +12 T, the longitudinal temperature difference  $\Delta T_i$  exhibits apparently symmetrical behavior, a large even signal accompanied by a tiny odd background. But the transverse temperature difference  $\Delta T_j$  is predominantly asymmetrical: A large odd signal is accompanied by a small even background. To separate the signal from the background, we performed symmetric and asymmetric processing for the longitudinal and transverse temperature difference, respectively. For symmetric processing we used  $(\Delta T_i(+B) + \Delta T_i(-B))/2l$ , here  $l$  is the length between two longitudinal thermocouples. For asymmetric processing we used  $(\Delta T_j(+B) - \Delta T_j(-B))/2w$ , here  $w$  is the length between two transverse thermocouples. The processed results are shown in Figure S1B. The even component in the transverse response may come from either a lateral misalignment together with the magnetothermal conductivity of the sample or from the magnetothermal power of thermocouples. Note that the odd-to-even ratio is less than 1 mK/1.95 K in longitudinal response and more than 4 mK/0.36 K (i.e.) 20 times larger in the transverse response. This confirms that the asymmetrized transverse signal is indeed the transverse thermal Hall gradient, which should be odd in magnetic field.



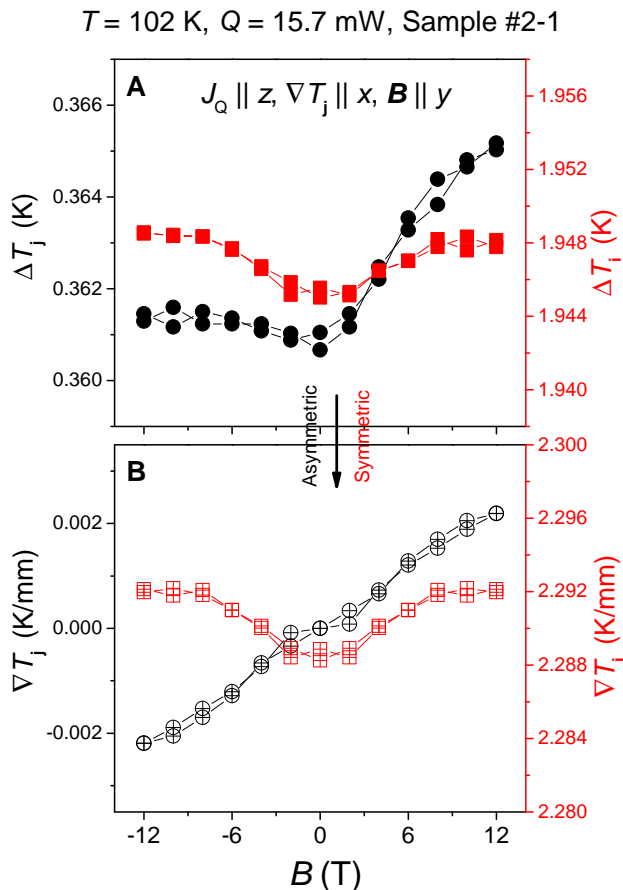


FIG. S1. **Raw data and its processing.** (A) The longitudinal and transverse temperature difference of sample #2-1 at 102 K under a heat power of 15.7 mW. (B) The results after the symmetric and asymmetric processing.

### S3. THE ANISOTROPIC DIELECTRIC CONSTANT OF BLACK P

BP has an anisotropic dielectric constant. Nagahama *et al.* [50] experimentally determined its amplitude of along three different orientation by optical means and found that it is 13 along zigzag direction, 16.5 along armchair direction and 8.3 for out-of-plane direction.

Valagiannopoulos *et al.* [42] calculated the real and imaginary parts of the dielectric constant in black P. The real components of their calculated values are in good agreement with what was measured [50] and show a modest anisotropy. Interestingly, there is a huge anisotropy in the imaginary component of the dielectric component along the two orientations (See the table). As a consequence, an electromagnetic wave is expected to be damped much less along the ‘zigzag’ direction compared to the ‘armchair’ direction.

	Re(armchair)	Re(zigzag)	Im(armchair)	Im(zigzag)
Theory [42]	18	14	0.45	0.04
experiment [50]	16.5	13	–	–

TABLE S2. Measured and calculated components of the dielectric tensor in black P along different orientations.

### S4. REPRODUCIBILITY

To ensure that the thermal Hall effect is intrinsic in black phosphorus, we repeated the measurements on other samples and used a different method. As seen in Figure S2B and Figure S3B, the thermal Hall effect was observed in two more samples #2-1 and #2-2. Their thermal Hall angle is anisotropic reflecting the anisotropy of the longitudinal thermal conductivity, as seen in Figure S2A and Figure S3A. In addition, we measured sample #2-2 using resistive thermometers instead of thermocouples and found a similar result, as seen in Figure S3C.

### S5. ROLE OF ELECTRONS IN THERMAL TRANSPORT

Figure S4A shows the resistivity of black phosphorus along different orientations. The electronic thermal conductivity  $\kappa_{xx}^e$  and  $\kappa_{zz}^e$  estimated from  $\rho_{xx}$  and  $\rho_{zz}$  through the Wiedemann-Franz law, is about 4 to 8 orders of magnitude smaller than the total thermal conductivity  $\kappa_{xx}$  and  $\kappa_{zz}$ , as seen in Figure S4B, implying that phonons dominate the thermal transport in Black phosphorus.

Figure S5A shows the temperature dependence of the three components of the electrical conductivity tensor. Figure S5B compares the electrical and the thermal Hall angle. In the whole temperature range, the former is three orders of magnitude larger than the latter. This can generate a phonon drag thermal Hall effect [16] provided that there is large momentum exchange between electrons and phonons.

Figure S5C compares the electronic thermal Hall conductivity estimated through the Wiedemann-Franz law and the measured thermal Hall conductivity. At low temperature they are separated by five orders of magnitude. On the other hand, at room temperature the difference is only one order of magnitude. Therefore, a sizeable difference between the zero-electric-current and the zero-electric field thermal conductivities can arise due to the thermoelectric component of the thermal Hall conductivity. This feature was documented in detail in the case of metallic strontium titanate. It would explain the observed inequality between  $\kappa_{ij}$  and  $\kappa_{ji}$  near room temperature, where electrons matter most.

Reproducibility in Sample #2-1.  $J_Q \parallel z$ ,  $\nabla T_j \parallel x$ ,  $\mathbf{B} \parallel y$

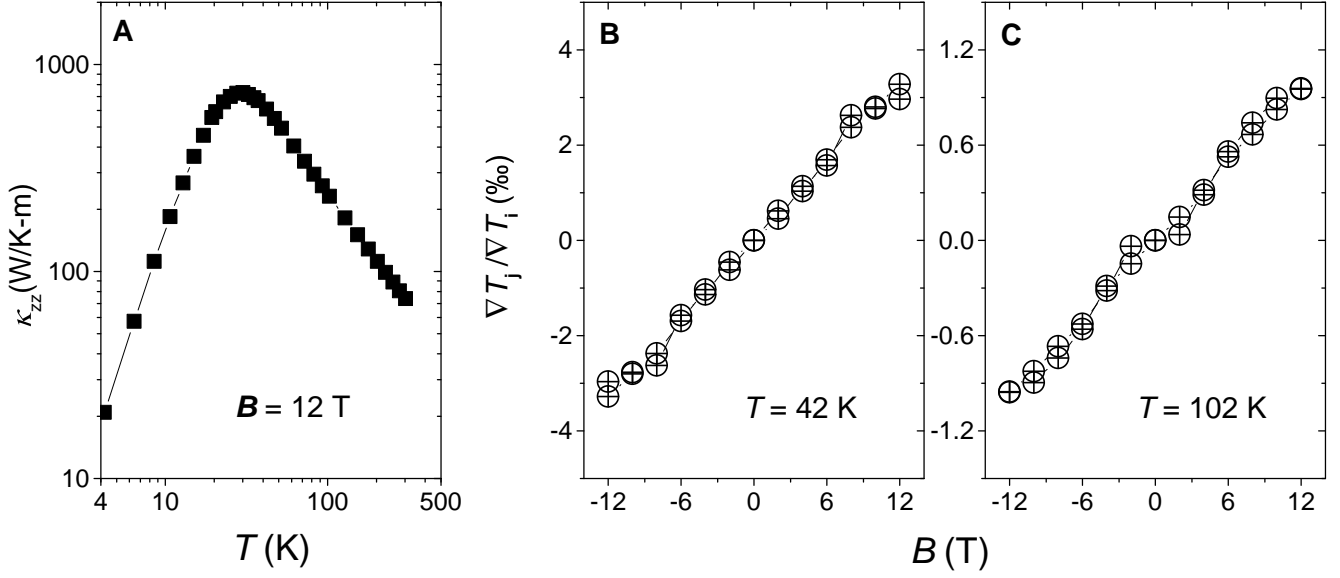


FIG. S2. **Reproducibility of thermal Hall effect in sample #2-1.** (A) The thermal conductivity of #2-1 along  $z$ -axis. (B-C) The thermal Hall angle of #2-1 at 42 K and 102 K.

### S6. THE MEAN FREE PATH OF PHONONS AND THE SAMPLE THICKNESS

Figure S6 shows the mean free path of phonons in different BP crystals with different thicknesses [37]. It was extracted from the longitudinal thermal conductivity, the sound velocity and the specific heat. The mean-free-path shows a non-monotonic temperature dependence as a re-

sult of the Poiseuille flow of phonons. As the thickness of the sample increases, the absolute value of thermal conductivity enhances. This implies that at least a sub-set of phonons travel across the sample without collision.

Note that near the peak temperature ( $\approx 30$  K), the mean free path remains well below the sample thickness, which indicates that boundary scattering is not dominant. Interbranch phonon coupling is the most plausible source of additional thermal resistivity.

Reproducibility of methods.  $J_Q \parallel x, \nabla T_j \parallel z, \mathbf{B} \parallel y$

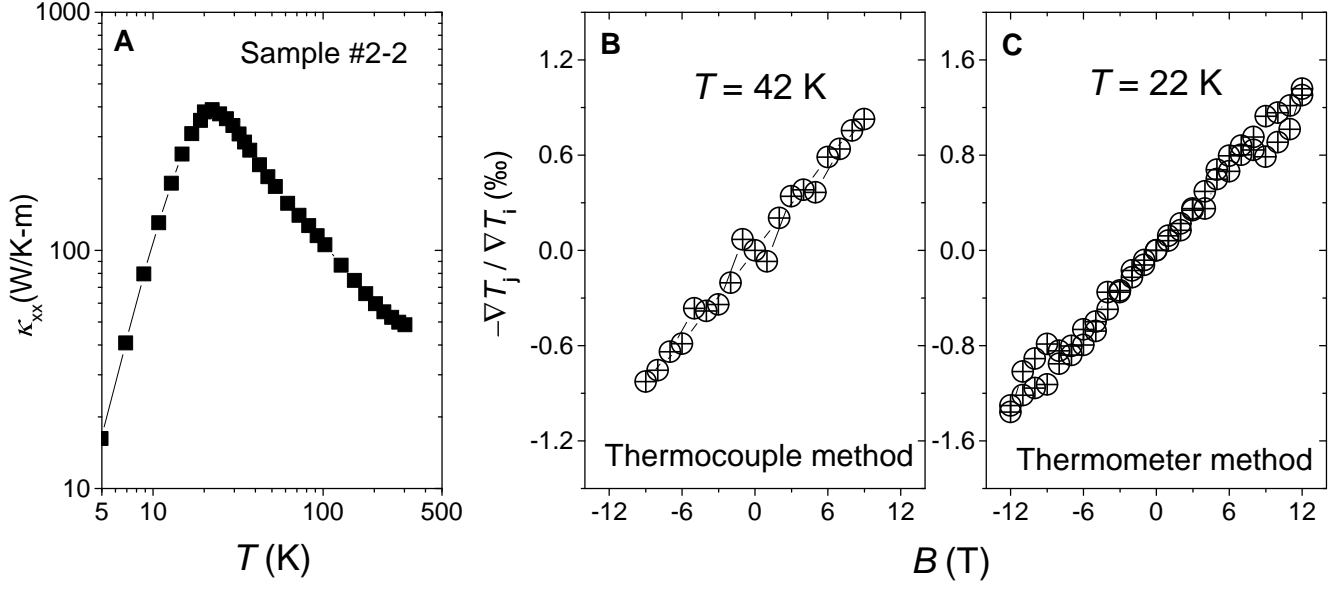


FIG. S3. **Reproducibility of thermal Hall effect in different methods.** (A) The thermal conductivity of #2-2 along  $x$ -axis by thermocouples method. (B) The thermal Hall angle of #2-2 at 42 K measured by the thermocouples method. (C) The thermal Hall angle of #2-2 at 22 K measured by the thermometers method.

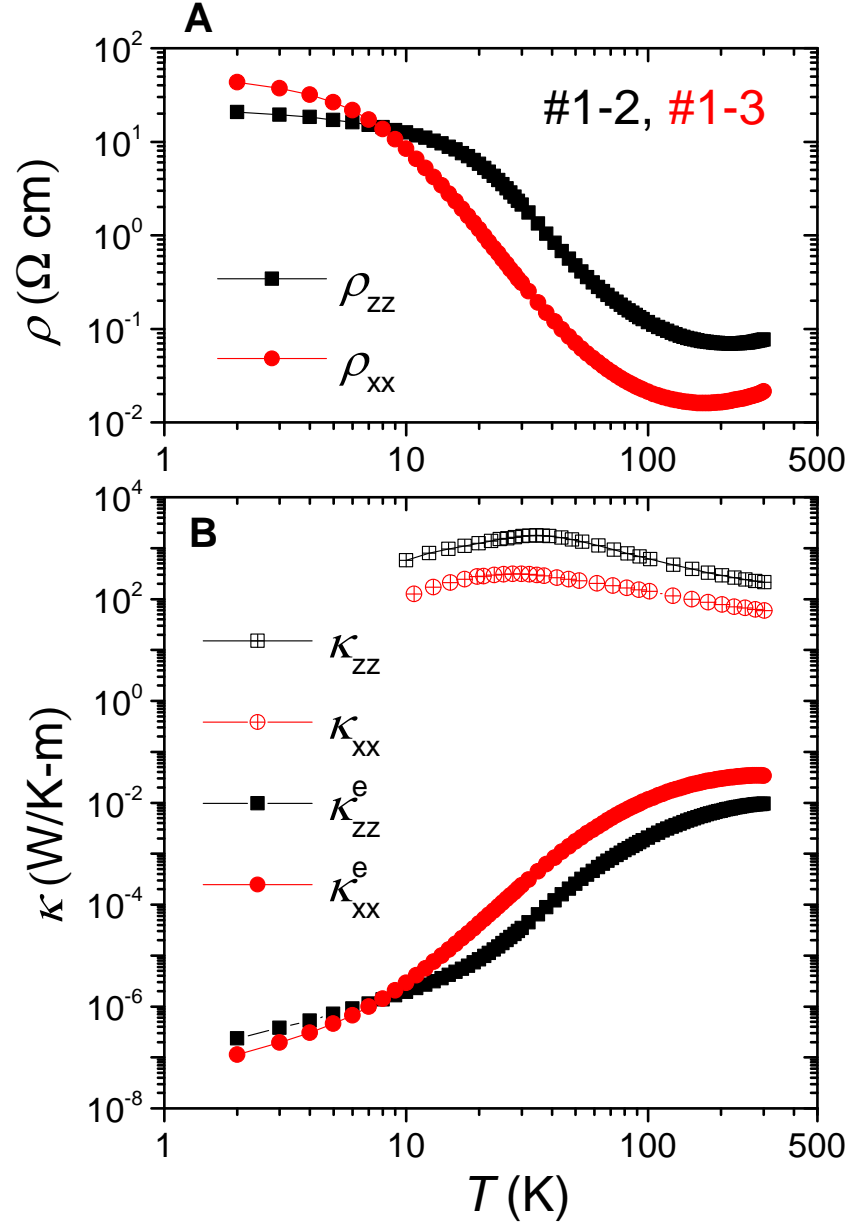


FIG. S4. **Resistivity and electron thermal conductivity.** (A) The  $\rho_{zz}$  measured in #1-2 and  $\rho_{xx}$  measured in #1-3. (B) The electron thermal conductivity  $\kappa_{xx}^e$  and  $\kappa_{zz}^e$  estimated through the Wiedemann-Franz law, compares with the total thermal conductivity  $\kappa_{xx}$  and  $\kappa_{zz}$  measured in #1-1.

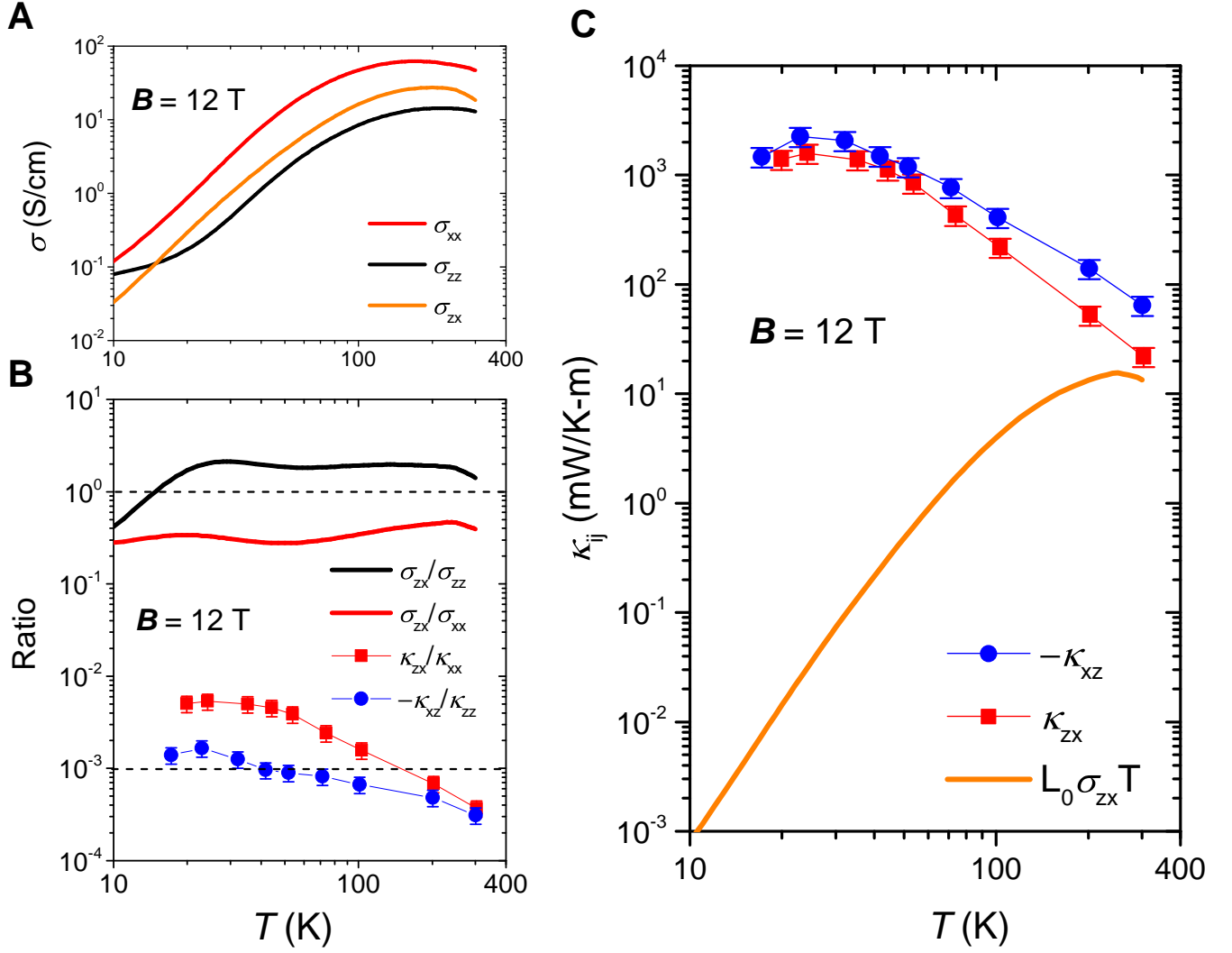


FIG. S5. **Phonon drag and a thermoelectric component at high temperature.** (A) Comparison of diagonal and off-diagonal electrical conductivity. (B) Comparison of the electrical Hall angle with their thermal counterparts. (C) Comparison of the electrical thermal Hall conductivity estimated through the Wiedemann-Franz law and the measured thermal Hall conductivity.

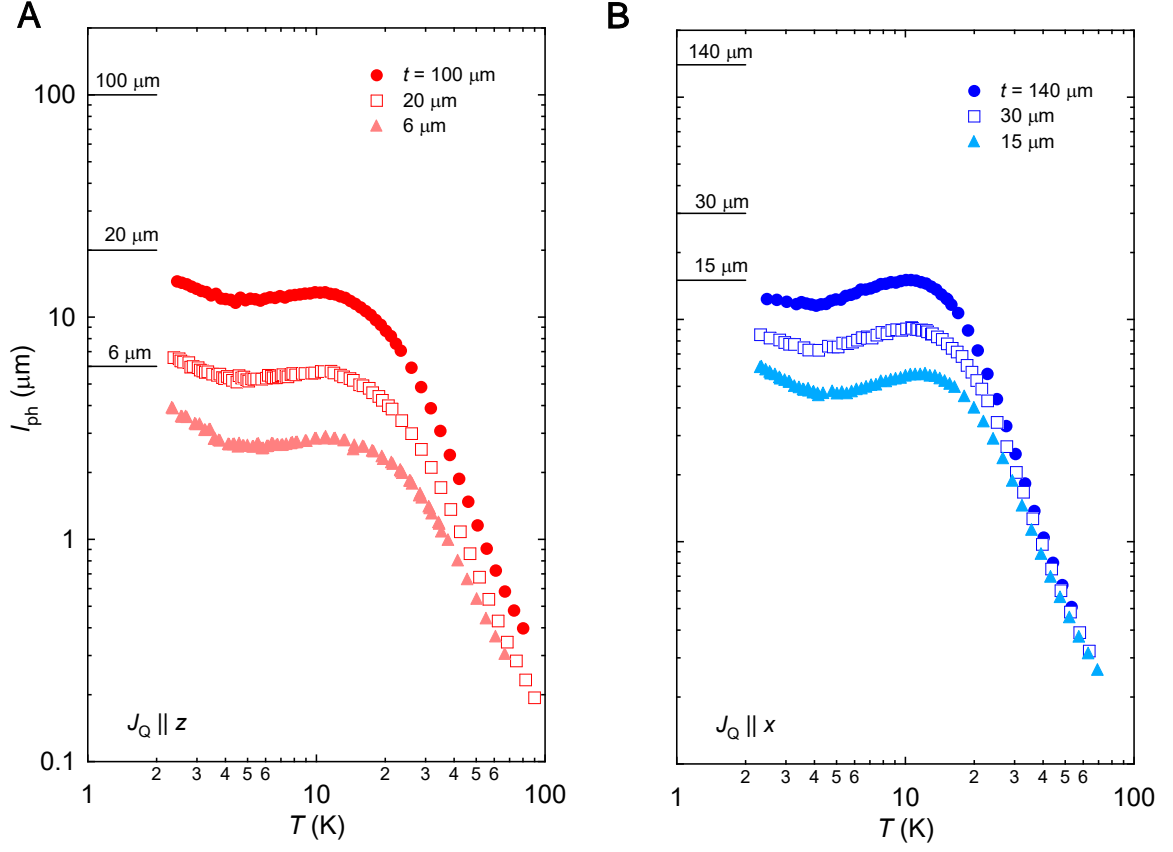


FIG. S6. **Mean-free-path of phonons in BP.** The mean-free-path of phonons in BP for both orientations for samples with different thicknesses [37]. The horizontal bars in the figure denote thickness of each sample. The mean-free-path increases with increasing thickness implying that a fraction of heat-carrying phonons are ballistic. But it remains well below the sample thickness indicating that there is another resistive process in addition to boundary scattering of acoustic phonons.